Deterministic conversions between Greenberger-Horne-Zeilinger states and *W* states of spin qubits via Lie-transform-based inverse Hamiltonian engineering

Yi-Hao Kang,[1] Zhi-Cheng Shi,[1] Bi-Hua Huang,[1] Jie Song,[2] and Yan Xia[1,*]
[1]*Department of Physics, Fuzhou University, Fuzhou 350002, China*
[2]*Department of Physics, Harbin Institute of Technology, Harbin 150001, China*

(Received 7 May 2019; published 22 July 2019)

In this paper, we propose a protocol to realize the conversions between Greenberger-Horne-Zeilinger (GHZ) states and *W* states of spin qubits. By analyzing and simplifying the dynamics of the system, the control fields are designed via the inverse Hamiltonian engineering based on the Lie transforms. Moreover, the states' conversions between multitype GHZ states and *W* states can be executed deterministically and reversibly, which makes the protocol resource saving and flexible. We show in numerical simulations that the state conversions are robust against the systematic errors, random noise, and frequency mismatching of the control fields. Therefore, the protocol may provide some useful prospectives to the research of quantum mechanics and applications of quantum information processing based on GHZ states and *W* states.

DOI: 10.1103/PhysRevA.100.012332

I. INTRODUCTION

Entanglement is a critical physical resource that plays a significant role in investigations of the fundamental theory of quantum mechanics and applications of quantum information processing (QIP) [1–4]. In the research of entanglement over the past decades, multiparticle entangled states have attracted great interest as they possess larger information capacity and can be used in performing quantum information tasks with more complexity [5,6]. Among all kinds of multiparticle entangled states, it has been shown that there exist two very important types of states, the Greenberger-Horne-Zeilinger (GHZ) states [7] and the *W* states [8]. These two types of entangled states have many practical uses in common. For example, both the GHZ states and the *W* states can be exploited in testing quantum mechanics against local hidden theory [9,10]. Besides, they are both very useful in quantum information tasks including quantum teleportation [11,12], quantum state sharing [13,14], quantum secure direct communication [15,16], and so on. On the other hand, the GHZ states and the *W* states possess their own features. The GHZ state is referred to as maximally entangled by many entanglement measures [17,18]. When the qubit loss happens to a GHZ state, the rest of the qubits would be in a mixed state with only classical correlations [19] while, for the *W* state, it holds robustness against qubit loss because of the symmetry, i.e., the remaining qubits can be still entangled if one qubit is lost [8]. In fact, the GHZ states and the *W* states are inequivalent classes of entangled states and impossible to convert to each other with only local operations and classical communication [19,20]. However, the requirements of the conversions between GHZ states and *W* states for different physical systems appear in many theoretic and experimental research works about entanglements and the applications of QIP [21–25], e.g., the state conversion between different types of entangled states is one of the important processes in forming complete toolboxes of physically realizable operations and gates in quantum networks [21]. Thus, the question of if it is possible to realize the conversions between GHZ states and *W* states naturally arises.

To date, much effort has been devoted to the conversions between GHZ states and *W* states [19,23–25] in different physical systems. Previous protocols [19,23] have shown that it is possible to convert GHZ states to *W* states, approximately, with the help of positive operator valued measures. As the state conversions are not deterministic in protocols [19,23], the physical resources may be wasted in the process. For protocol [19], there exists a trade-off between the successful probability and the fidelity of the target state, i.e., the rise of the fidelity causes the decrease of the successful probability. For protocol [23], the maximal successful probability is $3/4$, which is obtained in the ideal case with all the efficiencies of photon detectors being 1. To realize the deterministic conversions, protocols [24,25] with different techniques are proposed. In protocol [24], the conversions from GHZ states to *W* states with both the successful probability and the fidelity of obtaining *W* states are unity via the homodyne measurement. Protocol [25] has demonstrated that the conversions from *W* states to GHZ states can be realized successfully through dissipative dynamics processes. As the state conversions are both deterministic in protocols [24,25], the physical resources that may be wasted in the fail cases can be saved. However, as these protocols [24,25] are not based on a unitary evolution, the state conversions are irreversible. This may limit the applications of protocols [24,25] in some cases.

In this paper, inspired by time-reversal symmetry of the unitary dynamics of interacting qubits, we propose a protocol to realize deterministic and reversible conversions between GHZ states and *W* states. The physical system considered

*xia-208@163.com

here is the spin system, as it possess many advantages including long coherence time [26,27], good scalably [28,29], nice operability [30–32], capability of fast initialization and readout [33–35], and is widely used in the studies of entanglement [36,37] and various quantum information tasks [38–43]. Moreover, considering the fact that the dynamics of the spin system can be simulated by atom-cavity coupled systems [44], optical lattices [45], ion traps [46], polar molecules [47], superconducting circuits [48–50], etc., the protocol may also be extended for use in some other physical systems. On the other hand, the inverse Hamiltonian engineering [51–64] is considered as an important control method to design the unitary evolution, which allows us to design feasible control fields with robustness against parametric errors and noise [65,66]. Considering the dynamic symmetry of the spin system, the control fields can be designed via the Lie-transform-based inverse Hamiltonian engineering [64]. By properly selecting the boundary conditions of control parameters, we show that the conversions between multitype GHZ states and W states of three spin qubits can be successfully executed in only one step. Comparing with the multistep protocol [23] assisted by several Hadamard operations, the procedure in the current protocol is simpler. Moreover, with the control fields applied to the spin qubits, addressing the spin qubits is not needed in the state conversions, which may also relax the experimental requirement. At the end of the paper, we also analyze the performance of the state conversions under the influence of the experimental errors and imperfections, where the results demonstrate the protocol holds the robustness against different disturbing factors. Therefore, the protocol may be helpful to the fundamental research and the quantum information tasks with the GHZ states and the W states.

The paper is organized as follows. In Sec. II A, the Hamiltonian for the conversions between spin GHZ states and W states are presented. In Sec. II B, the method for the design of the control fields is put forward based on the derived effective Hamiltonian by combining inverse Hamiltonian engineering with Lie transforms. In Sec. II C, three examples of the state conversions are demonstrated to show the validity of the derived effective Hamiltonian and the control fields. In Sec. III, the performance of the protocol under the influence of experimental errors and imperfections are discussed via numerical simulations. Finally, the conclusion will be given in Sec. IV.

II. DETERMINISTIC CONVERSIONS BETWEEN GHZ STATES AND W STATES OF SPIN QUBITS VIA LIE-TRANSFORM-BASED INVERSE HAMILTONIAN ENGINEERING

A. The Hamiltonian for the conversions between GHZ states and W states of spin qubits

We consider the system consists three spin qubits denoted by 1, 2, 3, respectively. The spin operator of spin qubit k ($k = 1, 2, 3$) is $\vec{S}_k = S_x^{(k)}(t)\vec{e}_x + S_y^{(k)}(t)\vec{e}_y + S_z^{(k)}(t)\vec{e}_z$, with $\vec{e}_x$ ($\vec{e}_y$, $\vec{e}_z$) being the unit vector along the x axis (y axis, z axis). Besides, the gyromagnetic ratios are set as g for all spin qubits. The system is driven by a time-dependent magnetic field $\vec{B}(t) = B_x(t)\vec{e}_x + B_y(t)\vec{e}_y + B_z(t)\vec{e}_z$. Between each pair of spin qubits, there exists anisotropic Heisenberg interactions, where the coupling strengthes of the Heisenberg interactions between spin qubits k and k' ($k \neq k'$) are $J_x^{kk'}$, $J_y^{kk'}$, and $J_z^{kk'}$ for directions along x axis, y axis, and z axis, respectively. The Hamiltonian of the three-spin system can be described by ($\hbar = 1$)

$$H(t) = g\vec{B}(t)\cdot\left(\sum_{k=1}^{3}\vec{S}_k\right) + \sum_{k<k'}\left[J_x^{kk'}(t)S_x^{(k)}S_x^{(k')} + J_y^{kk'}(t)S_y^{(k)}S_y^{(k')} + J_z^{kk'}(t)S_z^{(k)}S_z^{(k')}\right]. \tag{1}$$

The anisotropic Heisenberg interactions and the tunable coupling strengthes of spin qubits have been observed and experimentally realized in previous schemes [40,67,68] with nuclear magnetic resonance (NMR) systems, nitrogen-vacancy centers in diamond, and quantum dots. Therefore, the Hamiltonian shown in Eq. (1) is feasible. By considering the symmetry of the GHZ states and the W states, we select $J_x^{kk'} = J_y^{kk'} = -J_z^{kk'}/2 = J$, and the three components of time-dependent magnetic field $\vec{B}(t)$ are chosen by

$$\begin{aligned} B_x(t) &= \sum_{j=1}^{3} B_j(t)\cos(\omega_j t + \phi_j), \\ B_y(t) &= \sum_{j=1}^{3} B_j(t)\sin(\omega_j t + \phi_j), \quad B_z(t) = 0, \end{aligned} \tag{2}$$

where ω_j is the rotation frequency of the magnetic component $B_j(t)$ around the z-axis, and ϕ_j is the initial phase of the rotation. When $\omega_j < 0$ ($\omega_j > 0$), the rotation is left-circular rotation (right-circular rotation). With the parameters selected above, the Hamiltonian shown in Eq. (1) becomes

$$\begin{aligned} H(t) &= H_0 + H_1(t), \\ H_0 &= -6J(|\uparrow\uparrow\uparrow\rangle\langle\uparrow\uparrow\uparrow| + |\downarrow\downarrow\downarrow\rangle\langle\downarrow\downarrow\downarrow| \\ &\quad - |W\rangle\langle W| - |W'\rangle\langle W'|), \\ H_1(t) &= \sum_{j=1}^{3} gB_j(t)e^{-i(\omega_j t+\phi_j)}[(\sqrt{3}|\uparrow\uparrow\uparrow\rangle\langle W| \\ &\quad + 3|W\rangle\langle W'| + \sqrt{3}|W'\rangle\langle\downarrow\downarrow\downarrow|) - (|\uparrow\uparrow\downarrow\rangle\langle\downarrow\downarrow\uparrow| \\ &\quad + |\uparrow\downarrow\uparrow\rangle\langle\downarrow\uparrow\downarrow| + |\downarrow\uparrow\uparrow\rangle\langle\uparrow\downarrow\downarrow|)] + \text{H.c.}, \end{aligned} \tag{3}$$

where $|W\rangle$ and $|W'\rangle$ are defined as

$$\begin{aligned} |W\rangle &= \frac{1}{\sqrt{3}}(|\uparrow\uparrow\downarrow\rangle + |\uparrow\downarrow\uparrow\rangle + |\downarrow\uparrow\uparrow\rangle), \ |W'\rangle \\ &= \frac{1}{\sqrt{3}}(|\uparrow\downarrow\downarrow\rangle + |\downarrow\downarrow\uparrow\rangle + |\downarrow\uparrow\downarrow\rangle). \end{aligned} \tag{4}$$

We consider the conditions $\omega_1 = -12J$, $\omega_2 = 0$, $\omega_3 = 12J$, and $|gB_j(t)| \ll J$. By performing a rotation with $R(t) = e^{-iH_0 t}$ and discarding terms with high frequency oscillations, the effective Hamiltonian can be derived as

$$\begin{aligned} H_e(t) &= \Omega_1(t)e^{-i\phi_1}|\uparrow\uparrow\uparrow\rangle\langle W| + \Omega_2(t)e^{-i\phi_2}|W\rangle\langle W'| \\ &\quad + \Omega_3(t)e^{-i\phi_3}|W'\rangle\langle\downarrow\downarrow\downarrow| + \text{H.c.}, \end{aligned} \tag{5}$$

TABLE I. The results of $-i[G_l, G_{l'}]$.

$G_{l'}$ \ G_l	G_1	G_2	G_3	G_4	G_5	G_6
G_1	0	0	$-G_5$	$-G_6$	G_3	G_4
G_2	0	0	G_6	G_5	$-G_4$	$-G_3$
G_3	G_5	$-G_6$	0	0	$-G_1$	G_2
G_4	G_6	$-G_5$	0	0	G_2	$-G_1$
G_5	$-G_3$	G_4	G_1	$-G_2$	0	0
G_6	$-G_4$	G_3	$-G_2$	G_1	0	0

with

$$\Omega_1(t) = \sqrt{3}gB_1(t),\ \Omega_2(t) = 2gB_2(t),\ \Omega_3(t) = \sqrt{3}gB_3(t). \tag{6}$$

Noticing that when the final states of the system are GHZ states $|\mathrm{GHZ}_\pm\rangle = \frac{1}{\sqrt{2}}(|\uparrow\uparrow\uparrow\rangle \pm |\downarrow\downarrow\downarrow\rangle)$ or W states $|W\rangle$ and $|W'\rangle$, the rotation $R(t)$ only induces global phases as e^{6iJt} (for GHZ states) and e^{-6iJt} (for W states), the state conversions between GHZ states and the W states can be discussed in the rotation frame of $R(t)$ up to global phases.

B. The design of control fields with Lie-transform-based inverse Hamiltonian engineering

We now describe the design of control fields with the effective Hamiltonian $H_e(t)$ in Eq. (5) by using the Lie-transform-based inverse Hamiltonian engineering [64]. A simple way to establish dynamic symmetry is to set $\phi_1 = -\phi_2$, such that $H_e(t)$ can be rewritten by

$$H_e(t) = \sum_{n=1}^{3} \Omega_n(t)|\xi_n\rangle\langle\xi_{n+1}| + \mathrm{H.c.}, \tag{7}$$

with $|\xi_1\rangle = |\uparrow\uparrow\uparrow\rangle$, $|\xi_2\rangle = e^{i\phi_1}|W\rangle$, $|\xi_3\rangle = |W'\rangle$, $|\xi_4\rangle = e^{i\phi_3}|\downarrow\downarrow\downarrow\rangle$. In this case, $H_e(t)$ can be described within SO(4) Lie algebra as

$$H_e(t) = \Omega_1(t)G_1 + \Omega_3(t)G_2 + \Omega_2(t)G_3 + 0(G_4 + G_5 + G_6), \tag{8}$$

with generators $\{G_l | l = 1, 2, \ldots, 6\}$ being

$$\begin{aligned} &G_1 = |\xi_1\rangle\langle\xi_2| + |\xi_2\rangle\langle\xi_1|,\ G_2 = |\xi_3\rangle\langle\xi_4| + |\xi_4\rangle\langle\xi_3|, \\ &G_3 = |\xi_2\rangle\langle\xi_3| + |\xi_3\rangle\langle\xi_2|,\ G_4 = |\xi_1\rangle\langle\xi_4| + |\xi_4\rangle\langle\xi_1|, \\ &G_5 = -i|\xi_1\rangle\langle\xi_3| + i|\xi_3\rangle\langle\xi_1|,\ G_6 = -i|\xi_2\rangle\langle\xi_4| + i|\xi_4\rangle\langle\xi_2|. \end{aligned} \tag{9}$$

The commutation relation between generators are shown in Table I.

By using the Lie-transform-based inverse Hamiltonian engineering, we define Lie transform $\mathscr{L}_l$ $(l = 1, 2, \ldots, 6)$ with time-dependent parameter θ_l, whose function acting on an arbitrary operator $A \in \mathcal{G} = \mathrm{span}\{G_l | l = 1, 2, \ldots, 6\}$ is

$$\mathscr{L}_j(A) = e^{i\theta_l(t)G_l} A e^{-i\theta_l(t)G_l}, \tag{10}$$

which can be described by matrices in basis $\{G_l | l = 1, 2, \ldots, 6\}$. Since the rotation $e^{-i\theta_l(t)G_l}$ can transform the Hamiltonian from a picture to another picture, we can define a picture transform acting on $H_e(t)$ as

$$\begin{aligned} \mathscr{P}_l(H_e) &= e^{i\theta_l(t)G_l} H_e e^{-i\theta_l(t)G_l} - ie^{i\theta_j(t)G_l}\frac{d}{dt}[e^{-i\theta_j(t)G_l}] \\ &= \mathscr{L}_l(H_e) - \dot{\theta}_l(t)G_l. \end{aligned} \tag{11}$$

According to the properties of the Lie transform, we have $\mathscr{L}_j(A) \in \mathcal{G}$ when $A \in \mathcal{G}$. Thus, $\mathscr{P}_l(H_e) \in \mathcal{G}$ is also satisfied, such that the result of the compound picture transform $\mathscr{P}_{l'} \circ \mathscr{P}_l(H_e) = \mathscr{P}_{l'}[\mathscr{P}_l(H_e)]$ is also a Hermitian operator in $\mathcal{G}$. In general, we can perform the compound picture transform as

$$\mathscr{P}_6 \circ \cdots \circ \mathscr{P}_2 \circ \mathscr{P}_1 \tag{12}$$

on H_e, and obtain

$$\begin{aligned} &\mathscr{P}_6 \circ \cdots \circ \mathscr{P}_2 \circ \mathscr{P}_1(H_e) \\ &= \mathscr{L}_6 \circ \cdots \circ \mathscr{L}_2 \circ \mathscr{L}_1(H_e) - \dot{\theta}_1(t)\mathscr{L}_6 \circ \cdots \circ \mathscr{L}_3 \circ \mathscr{L}_2(G_1) \\ &\quad -\dot{\theta}_2(t)\mathscr{L}_6 \circ \cdots \circ \mathscr{L}_4 \circ \mathscr{L}_3(G_2) - \dot{\theta}_3(t)\mathscr{L}_6 \circ \mathscr{L}_5 \circ \mathscr{L}_4(G_3) \\ &\quad -\dot{\theta}_4(t)\mathscr{L}_6 \circ \mathscr{L}_5(G_4) - \dot{\theta}_5(t)\mathscr{L}_5(G_5) - \dot{\theta}_6(t)G_6. \end{aligned} \tag{13}$$

When the condition

$$\mathscr{P}_6 \circ \cdots \circ \mathscr{P}_2 \circ \mathscr{P}_1(H_e) = 0 \tag{14}$$

is satisfied, the evolution operator $U_e(t)$ for the evolution governed by $H_e(t)$ satisfied

$$U(t) = e^{-i\theta_1(t)G_1} e^{-i\theta_2(t)G_2} \cdots e^{-i\theta_6(t)G_6} e^{i\theta_6(0)G_6} e^{i\theta_5(0)G_5} \cdots e^{i\theta_1(0)G_1}, \tag{15}$$

as the compound picture transform in Eq. (12) is equivalent to the picture transform defining the evolution operator $U_e(t)$, i.e.,

$$\mathscr{P}_{U_e}(H_e) = U_e^\dagger(t)H_e(t)U_e(t) - iU_e^\dagger(t)\dot{U}e(t) = 0, \tag{16}$$

with the Schrödinger equation $i\dot{U}_e(t) = H_e(t)U_e(t)$ being used. In this case, both the evolution operator $U_e(t)$ and the Hamiltonian $H_e(t)$ are associated with parameters $\{\theta_l(t) | l = 1, 2, \ldots, 6\}$. On one hand, the evolution operator U_e can be calculated from Eq. (15) as $U_e(t) = U_\theta(t)U_\theta^\dagger(0)$ in basis $\{|\xi_1\rangle, |\xi_2\rangle, |\xi_3\rangle, |\xi_4\rangle\}$ with

$$U_\theta(t) = \begin{bmatrix} \cos\theta_1\cos\theta_4\cos\theta_5 - \sin\theta_1\sin\theta_3\sin\theta_5 & -i(\cos\theta_3\cos\theta_6\sin\theta_1 + \cos\theta_1\sin\theta_4\sin\theta_6) \\ -i(\cos\theta_4\cos\theta_5\sin\theta_1 + \cos\theta_1\sin\theta_3\sin\theta_5) & \cos\theta_1\cos\theta_3\cos\theta_6 - \sin\theta_1\sin\theta_4\sin\theta_6 \\ \cos\theta_2\cos\theta_3\sin\theta_5 - \cos\theta_5\sin\theta_2\sin\theta_4 & -i(\cos\theta_2\cos\theta_6\sin\theta_3 + \cos\theta_4\sin\theta_2\sin\theta_6) \\ -i(\cos\theta_2\cos\theta_5\sin\theta_4 + \cos\theta_3\sin\theta_2\sin\theta_5) & \cos\theta_2\cos\theta_4\sin\theta_6 - \cos\theta_6\sin\theta_2\sin\theta_3 \end{bmatrix}$$

$$\begin{bmatrix} -\cos\theta_5\sin\theta_1\sin\theta_3 - \cos\theta_1\cos\theta_4\sin\theta_5 & -i(\cos\theta_1\cos\theta_6\sin\theta_4 - \cos\theta_3\sin\theta_1\sin\theta_6) \\ -i(\cos\theta_1\cos\theta_5\sin\theta_3 - \cos\theta_4\sin\theta_1\sin\theta_5) & -\cos\theta_6\sin\theta_1\sin\theta_4 - \cos\theta_1\cos\theta_3\sin\theta_6 \\ \cos\theta_2\cos\theta_3\cos\theta_5 + \sin\theta_2\sin\theta_4\sin\theta_5 & -i(\cos\theta_4\cos\theta_6\sin\theta_2 - \cos\theta_2\sin\theta_3\sin\theta_6) \\ -i(\cos\theta_3\cos\theta_5\sin\theta_2 - \cos\theta_2\sin\theta_4\sin\theta_5) & \cos\theta_2\cos\theta_4\cos\theta_6 + \sin\theta_2\sin\theta_3\sin\theta_6 \end{bmatrix}. \quad (17)$$

Assuming the initial state of the system is $|\psi_0\rangle$, if the condition $U_\theta^\dagger(0)|\psi_0\rangle = |\xi_1\rangle$ is satisfied, the evolution of the system can be expressed by

$$\begin{aligned} |\psi_e(t)\rangle &= U_e(t)|\psi_0\rangle \\ &= (\cos\theta_1\cos\theta_4\cos\theta_5 - \sin\theta_1\sin\theta_3\sin\theta_5)|\uparrow\uparrow\uparrow\rangle \\ &\quad + (\sin\theta_1\cos\theta_4\cos\theta_5 + \cos\theta_1\sin\theta_3\sin\theta_5)|W\rangle \\ &\quad + (\cos\theta_2\cos\theta_3\sin\theta_5 - \sin\theta_2\sin\theta_4\cos\theta_5)|W'\rangle \\ &\quad + (\cos\theta_2\sin\theta_4\cos\theta_5 + \sin\theta_2\cos\theta_3\sin\theta_5)|\downarrow\downarrow\downarrow\rangle, \end{aligned} \quad (18)$$

with $\phi_1 = \phi_3 = \pi/2$ being set.

On the other hand, by reversely solving Eq. (14), the control fields $\Omega_1(t)$, $\Omega_2(t)$ and $\Omega_3(t)$ can be expressed by the functions of $\{\theta_l(t)\}$ as

$$\begin{aligned} \Omega_1(t) &= \dot\theta_1 + \dot\theta_5\sin\theta_3\cos\theta_4 + \dot\theta_6\cos\theta_3\sin\theta_4, \\ \Omega_2(t) &= \dot\theta_3\cos\theta_1\cos\theta_2 + \dot\theta_4\sin\theta_1\sin\theta_2 \\ &\quad - \dot\theta_5(\sin\theta_1\cos\theta_2\cos\theta_3\cos\theta_4 \\ &\quad + \cos\theta_1\sin\theta_2\sin\theta_3\sin\theta_4) \\ &\quad + \dot\theta_6(\cos\theta_1\sin\theta_2\cos\theta_3\cos\theta_4 \\ &\quad + \sin\theta_1\cos\theta_2\sin\theta_3\sin\theta_4), \\ \Omega_3(t) &= \dot\theta_2 - \dot\theta_5\cos\theta_3\sin\theta_4 - \dot\theta_6\sin\theta_3\cos\theta_4, \end{aligned} \quad (19)$$

with three constraint equations:

$$\begin{aligned} \dot\theta_4 &= \dot\theta_3\tan\theta_1\tan\theta_2, \\ \dot\theta_5 &= \frac{2\dot\theta_3(\sin\theta_3\sin\theta_4\tan\theta_2 - \cos\theta_3\cos\theta_4\tan\theta_1)}{\cos 2\theta_3 + \cos 2\theta_4}, \\ \dot\theta_6 &= \frac{2\dot\theta_3(\cos\theta_3\cos\theta_4\tan\theta_2 - \sin\theta_3\sin\theta_4\tan\theta_1)}{\cos 2\theta_3 + \cos 2\theta_4}. \end{aligned} \quad (20)$$

Therefore, one can first determine the boundary conditions for $\{\theta_l | l = 1, 2, \ldots, 6\}$ from Eq. (18) according to the initial states and the target states in the state conversions. Then, based on the determined boundary conditions, the time dependence of $\{\theta_l | l = 1, 2, \ldots, 6\}$ can be designed through proper functions, such as the polynomials or the trigonometric functions. Finally, the control fields can be obtained from Eqs. (19) and (20).

C. Examples for the state conversions

Until now, we have presented the effective Hamiltonian and the method of design of control fields for the state conversions. To show the validity and the flexibility of the protocol, we take the conversions between (i) $|\mathrm{GHZ}_+\rangle$ and $|W\rangle$, (ii) $|\mathrm{GHZ}_+\rangle$ and $|W'\rangle$, (iii) $|\mathrm{GHZ}_-\rangle$ and $|W\rangle$ as examples in the following subsections. The total interaction time for each state conversion process is assumed as T in the discussions afterward.

1. The conversions between $|GHZ_+\rangle$ and $|W\rangle$

According to Eq. (18), to convert the GHZ state $|\mathrm{GHZ}_+\rangle$ to the W state $|W\rangle$, the boundary conditions can be set as

$$\begin{aligned} &\theta_1(0) = \theta_1(T) = 0, \quad \theta_2(0) = 0, \quad \theta_3(T) = \pi/2, \\ &\theta_4(0) = \pi/4, \quad \theta_5(0) = 0, \quad \theta_5(T) = \pi/2. \end{aligned} \quad (21)$$

The simplest choice for $\theta_2(t)$ to fulfill Eqs. (21) is $\theta_2(t) = 0$, which gives the $\theta_4(t) = \pi/4$. According to Eqs. (20) and (21), Eq. (19) can be simplified as

$$\begin{aligned} \Omega_1(t) &= \dot\theta_1 - \dot\theta_3\tan\theta_1\tan 2\theta_3, \\ \Omega_2(t) &= \frac{\dot\theta_3}{\cos\theta_1}, \quad \Omega_3(t) = \frac{\dot\theta_3\tan\theta_1}{\cos 2\theta_3}. \end{aligned} \quad (22)$$

To make the control fields vanish at boundary, we add the condition as

$$\dot\theta_1(0) = \dot\theta_1(T) = \dot\theta_3(0) = \dot\theta_3(T) = 0. \quad (23)$$

Then, based on Eqs. (21) and (23), $\theta_1(t)$ and $\theta_3(t)$ can be designed as

$$\begin{aligned} \theta_1(t) &= -\Gamma_1\sin\left(\frac{\pi t}{T}\right)\sin\left(\frac{2\pi t}{T}\right), \\ \theta_3(t) &= \pi/2 + \Gamma_3\sin^2\left(\frac{\pi t}{T}\right), \end{aligned} \quad (24)$$

where Γ_1 and Γ_3 are two time-independent parameters to make

$$\theta_5(T) = -\int_0^T \frac{\sqrt{2}\dot\theta_3(t)\cos[\theta_3(t)]\tan[\theta_1(t)]}{\cos[2\theta_3(t)]}dt = \pi/2 \quad (25)$$

satisfied. By numerically calculating Eq. (25), the dependency relationship between Γ_1 and Γ_3 can be obtained, which is shown in Fig. 1(a). According to Fig. 1(a), we choose $\Gamma_1 = 0.35\pi$ and $\Gamma_3 = 0.2380\pi$ for control fields with appropriate amplitudes. With the chosen Γ_1 and Γ_3, $\Omega_1(t)$, $\Omega_2(t)$, and $\Omega_3(t)$ versus t/T are plotted in Fig. 1(b). Assuming the density operator is $\rho(t)$, we plot the population $P_W(t) = \langle W|\rho(t)|W\rangle$ of W state $|W\rangle$ and the population $P_+ = \langle \mathrm{GHZ}_+|\rho(t)|\mathrm{GHZ}_+\rangle$ of GHZ state $|\mathrm{GHZ}_+\rangle$ versus t/T by considering both the effective Hamiltonian $H_e(t)$ and the full Hamiltonian $H(t)$ with $J = 50/T$ in Fig. 1(c). As seen from Fig. 1(c), the evolution governed by the full Hamiltonian $H(t)$ matches with that governed by the effective Hamiltonian $H_e(t)$ very well up to small oscillations. The infidelity of the conversion from $|\mathrm{GHZ}_+\rangle$ to $|W\rangle$ is $1 - P_W^{\mathrm{full}}(T) = 7.8964 \times 10^{-5}$ with full Hamiltonian $H(t)$ and $J = 50/T$. The result shows the effective Hamiltonian derived in Sec. II A and the control fields designed in Sec. II B are both valid.

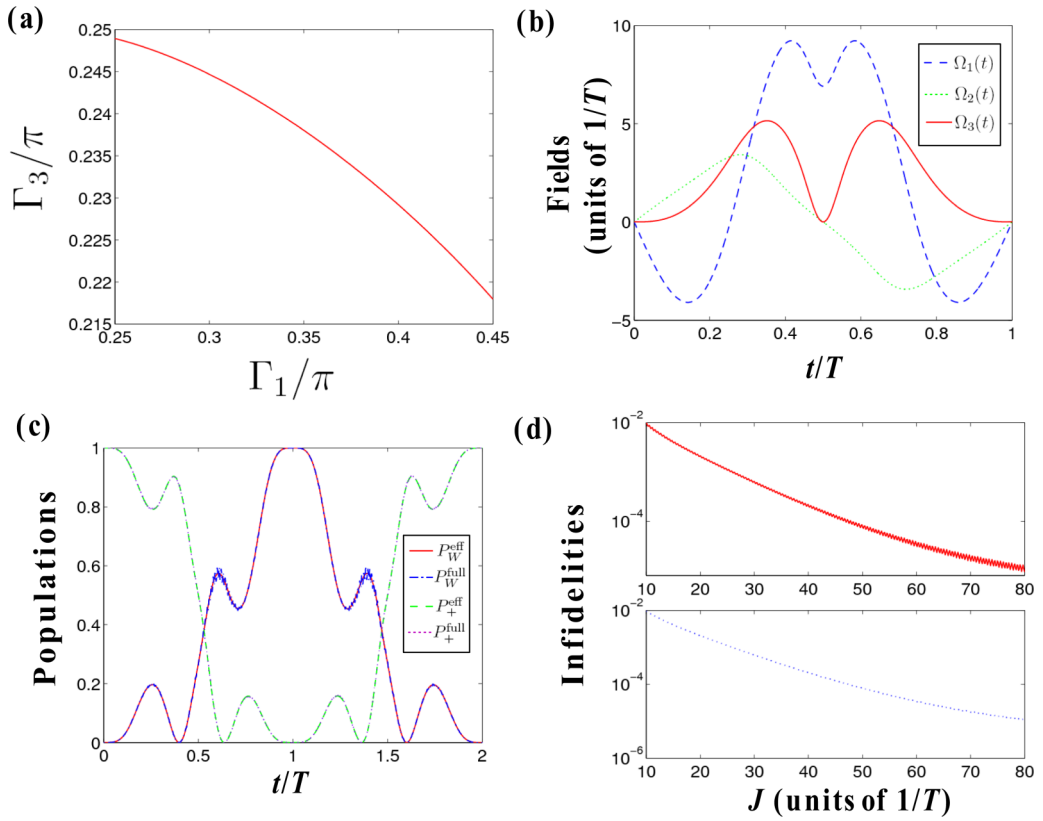

FIG. 1. (a) Γ_3/π versus Γ_1/π. (b) $\Omega_1(t)$, $\Omega_2(t)$, and $\Omega_3(t)$ versus t/T for $t \in [0, T]$. (c) The population $P_W^{\rm eff}(t)$ $[P_W^{\rm full}(t)]$ of W state $|W\rangle$ and the population $P_+^{\rm eff}(t)$ $[P_+^{\rm full}(t)]$ of GHZ state $|{\rm GHZ}_+\rangle$ with effective (full) Hamiltonian $H_e(t)$ $[H(t)]$ versus t/T, where $J = 50/T$ is set for the full Hamiltonian $H(t)$. The red solid line: $P_W^{\rm eff}(t)$; the blue dashed-dotted line: $P_W^{\rm full}(t)$; the green dashed line: $P_+^{\rm eff}(t)$; and the purple dotted line: $P_+^{\rm full}(t)$. (d) The red solid line: The infidelity of the conversion from $|{\rm GHZ}_+\rangle$ to $|W\rangle$ versus J; the blue dashed line: the infidelity of the conversion from $|W\rangle$ to $|{\rm GHZ}_+\rangle$ versus J.

To show that the conversion from $|W\rangle$ to $|{\rm GHZ}_+\rangle$ is also possible with the protocol, we consider the parameters with the following boundary conditions in the time interval $[T, 2T]$ as

$$\theta_1(T) = \theta_1(2T) = 0, \quad \theta_2(2T) = 0, \quad \theta_3(T) = \pi/2,$$
$$\theta_4(2T) = \pi/4, \quad \theta_5(T) = \pi/2, \quad \theta_5(2T) = 0. \tag{26}$$

A simple choice for parameters in time interval $[T, 2T]$ is $\theta_2(t) = 0$, $\theta_4(t) = \pi/4$, and

$$\theta_1(t) = -\theta_1(t - T), \ \theta_3(t) = \theta_3(t - T). \tag{27}$$

Then, according to Eq. (25), we have

$$\begin{aligned}\theta_5(2T) &= \theta_5(T) - \int_T^{2T} \frac{\sqrt{2}\dot{\theta}_3(t)\cos[\theta_3(t)]\tan[\theta_1(t)]}{\cos[2\theta_3(t)]}dt \\ &= \pi/2 + \int_T^{2T} \frac{\sqrt{2}\dot{\theta}_3(t-T)\cos[\theta_3(t-T)]\tan[\theta_1(t-T)]}{\cos[2\theta_3(t-T)]}dt \\ &= \pi/2 + \int_0^{T} \frac{\sqrt{2}\dot{\theta}_3(t)\cos[\theta_3(t)]\tan[\theta_1(t)]}{\cos[2\theta_3(t)]}dt = 0.\end{aligned} \tag{28}$$

Thus, with the above parameter selections for time interval $[T, 2T]$, all the boundary conditions in Eqs. (26) are fulfilled, and the fields for the conversion from $|W\rangle$ to $|{\rm GHZ}_+\rangle$ are $\Omega_1(t) = -\Omega_1(t - T)$, $\Omega_2(t) = \Omega_2(t - T)$, and $\Omega_3(t) = -\Omega_3(t - T)$ for $t \in [T, 2T]$. $P_W(t)$ and $P_+(t)$ versus t/T for $t \in [T, 2T]$ are also plotted in Fig. 1(c), by using the effective Hamiltonian $H_e(t)$ and the full Hamiltonian $H(t)$ with $J = 50/T$. Similar to the conversion from $|{\rm GHZ}_+\rangle$ to $|W\rangle$, the evolution governed by the full Hamiltonian $H(t)$ in time interval $[T, 2T]$ also matches well with that governed by the effective Hamiltonian $H_e(t)$, and the infidelity of the conversion is $1 - P_+^{\rm full}(2T) = 7.8841 \times 10^{-5}$. Therefore,

both the conversions from $|\mathrm{GHZ}_+\rangle$ to $|W\rangle$ and from $|W\rangle$ to $|\mathrm{GHZ}_+\rangle$ can be successfully completed with high fidelities in the protocol.

On the other hand, to investigate the performance of the conversions between $|\mathrm{GHZ}_+\rangle$ and $|W\rangle$ with different coupling strength J, we plot the infidelities of the conversion from $|\mathrm{GHZ}_+\rangle$ to $|W\rangle$ and the conversion from $|W\rangle$ to $|\mathrm{GHZ}_+\rangle$ versus J in Fig. 1(d). According to Fig. 1(d), the fidelities of the conversions between $|\mathrm{GHZ}_+\rangle$ and $|W\rangle$ are nearly 1 with $J \geqslant 10/T$. Even when $J = 10/T$, the fidelities of the conversions between $|\mathrm{GHZ}_+\rangle$ and $|W\rangle$ are higher than 0.9901. We can also find that the fidelities of the conversions between $|\mathrm{GHZ}_+\rangle$ and $|W\rangle$ have positive growth trends when J increases with small oscillations. That is because the evolution governed by the full Hamiltonian $H(t)$ approaches that governed by the effective Hamiltonian $H_e(t)$ gradually when J becomes larger and larger, assuming there exist two selections of coupling strengthes for the state conversions as $J_1 = K_1/T$ and $J_2 = K_2/T$. Besides, we suppose the maximal coupling strength that can be achieved in experiment is $J_{\max}$. Then, the shortest total interaction times for the two groups of state conversions are $T_{s1} = K_1/J_{\max}$ and $T_{s2} = K_2/J_{\max}$, respectively. Thus, although the fidelity of the state conversion may increase when one selects a large parameter $K = JT$, the lowest limit of total interaction time would also increase. Therefore, in experiments, one should make a trade-off between the fidelity and the interaction time according to the specific experimental conditions. As an example, let us make some numerical discussions about how to select K for the shortest time to obtain a fidelity for the conversion from $|\mathrm{GHZ}_+\rangle$ to $|W\rangle$ higher than a desired value F_s. By using the curve fitting on the red-solid line of Fig. 1(d), the infidelity of the conversion from $|\mathrm{GHZ}_+\rangle$ to $|W\rangle$ can be approximately described by a function $\Upsilon(K) = 1.012\exp[-(K+64.41)^2/34.04^2]$, which decreases when K increases. Assuming that the decoherence time of the system is τ, the total interaction time and the chosen value of K should satisfy $K/J_{\max} \leqslant T \leqslant \tau$. Thus, the considered F_s should not be higher than 1-$\Upsilon(J_{\max}\tau)$. As the effect of the decoherence may be ignorable when the total interaction time approaches the decoherence time, one may use an experimentally feasible time τ' instead of τ in the discussions. Considering a group of parameters $J_{\max} \simeq 100$ MHz, $\tau \simeq 1$s, $\tau' \simeq 10$ms in a NMR system [30,68], since $J_{\max}\tau \simeq 10^5$, $J_{\max}\tau' \simeq 10^3$, K, and F_s can take a value in a very large range. If we consider $F_s = 0.999$, the smallest value for K is $K_s = \Upsilon^{-1}(1-F_s) \simeq 25.13$, and the shortest total interaction time for obtaining a fidelity of the conversion from $|\mathrm{GHZ}_+\rangle$ to $|W\rangle$ higher than F_s is $T_s = K_s/J_{\max} \simeq 0.25$ms. If $F_s = 0.9999$ is considered, we have $K_s = \Upsilon^{-1}(1-F_s) \simeq 38.96$, $T_s = K_s/J_{\max} \simeq 0.39$ ms.

2. *The conversions between $|GHZ_+\rangle$ and $|W'\rangle$*

In Sec. II C 1, we described the design of boundary conditions and the selection of parameters for the conversions between $|\mathrm{GHZ}_+\rangle$ and $|W\rangle$ in detail. As the procedure is similar, here we only make brief descriptions on the realization of the conversions between $|\mathrm{GHZ}_+\rangle$ and $|W'\rangle$. According to Eq. (18), the boundary conditions of parameters for the conversion from $|\mathrm{GHZ}_+\rangle$ to $|W'\rangle$ are set as

$$\theta_1(0) = 0, \quad \theta_2(0) = \theta_2(T) = 0, \quad \theta_3(T) = 0,$$
$$\theta_4(0) = \pi/4, \quad \theta_5(0) = 0, \quad \theta_5(T) = \pi/2. \tag{29}$$

Similar to the parameter selection for the conversion from $|\mathrm{GHZ}_+\rangle$ to $|W\rangle$ in Sec. II C 1, the parameters selected for the conversion from $|\mathrm{GHZ}_+\rangle$ to $|W'\rangle$ are

$$\theta_1(t) = 0, \quad \theta_2(t) = \Gamma_2' \sin\left(\frac{\pi t}{T}\right)\sin\left(\frac{2\pi t}{T}\right),$$
$$\theta_3(t) = \Gamma_3' \sin^2\left(\frac{\pi t}{T}\right), \quad \theta_4(t) = \pi/4, \tag{30}$$

with Γ_2' and Γ_3' being two time-independent parameters to make

$$\theta_5(T) = \int_0^T \frac{\sqrt{2}\dot{\theta}_3(t)\sin[\theta_3(t)]\tan[\theta_2(t)]}{\cos[2\theta_3(t)]}dt = \pi/2, \tag{31}$$

satisfied. Besides, the control fields are given by

$$\Omega_1(t) = \frac{\dot{\theta}_3\tan\theta_2}{\cos 2\theta_3}, \quad \Omega_2(t) = \frac{\dot{\theta}_3}{\cos\theta_2},$$
$$\Omega_3(t) = \dot{\theta}_2 - \dot{\theta}_3\tan\theta_2\tan 2\theta_3. \tag{32}$$

With the selections of parameters as that in Eqs. (30), the curve of dependency relationship between Γ_2' and Γ_3' is the same as that shown in Fig. 1(a), i.e., one can substitute the (Γ_1/π) axis and (Γ_3/π) axis by (Γ_2'/π) axis and (Γ_3'/π) axis, respectively, to obtain the curve for Γ_3'/π versus Γ_2'/π. Therefore, $\Gamma_2' = 0.35\pi$ and $\Gamma_3' = 0.2380\pi$ are set for the control fields with appropriate amplitudes, which gives the time variations of $\Omega_1(t)$, $\Omega_2(t)$, and $\Omega_3(t)$ as shown in Fig. 2(a). We plot the population $P_{W'}(t) = \langle W'|\rho(t)|W'\rangle$ of W state $|W'\rangle$ and the population P_+ of GHZ state $|\mathrm{GHZ}_+\rangle$ versus t/T by using both the effective Hamiltonian $H_e(t)$ and the full Hamiltonian $H(t)$ and $J = 50/T$ in the Fig. 2(b). According to Fig. 2(b), the evolutions governed by the effective Hamiltonian $H_e(t)$ and full Hamiltonian $H(t)$ also match well with each other. The infidelity of the conversion from $|\mathrm{GHZ}_+\rangle$ to $|W'\rangle$ reads $1 - P_{W'}^{\mathrm{full}}(T) = 7.9031 \times 10^{-5}$. Thus, the conversion from $|\mathrm{GHZ}_+\rangle$ to $|W'\rangle$ is nearly perfect.

Similarly, we also set a group of boundary conditions for time interval $[T, 2T]$ for the conversion from $|W'\rangle$ to $|\mathrm{GHZ}_+\rangle$ as

$$\theta_1(2T) = 0, \quad \theta_2(T) = \theta_2(2T) = 0, \quad \theta_3(T) = 0,$$
$$\theta_4(2T) = \pi/4, \quad \theta_5(T) = \pi/2, \quad \theta_5(2T) = 0, \tag{33}$$

which leads the parameter selections as

$$\theta_1(t) = 0, \quad \theta_2(t) = -\theta_2(t-T),$$
$$\theta_3(t) = \theta_3(t-T), \quad \theta_4(t) = \pi/4. \tag{34}$$

It is easy to prove

$$\theta_5(2T) = \theta_5(T) + \int_T^{2T} \frac{\sqrt{2}\dot{\theta}_3(t)\sin[\theta_3(t)]\tan[\theta_2(t)]}{\cos[2\theta_3(t)]}dt = 0, \tag{35}$$

thus the boundary condition for θ_5 is also satisfied. Besides, the control fields in time interval $[T, 2T]$ are $\Omega_1(t) = -\Omega_1(t-T)$, $\Omega_2(t) = \Omega_2(t-T)$, and $\Omega_3(t) = -\Omega_3(t-T)$.

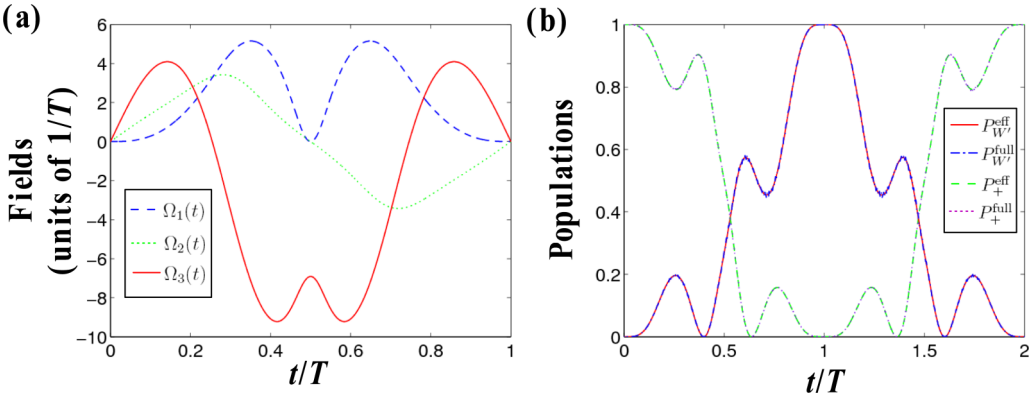

FIG. 2. (a) $\Omega_1(t)$, $\Omega_2(t)$, and $\Omega_3(t)$ versus t/T for $t \in [0, T]$. (b) The population $P^{\rm eff}_{W'}(t)$ $[P^{\rm full}_{W'}(t)]$ of W state $|W'\rangle$ and the population $P^{\rm eff}_{+}(t)$ $(P^{\rm full}_{+}(t))$ of GHZ state $|{\rm GHZ}_+\rangle$ with effective (full) Hamiltonian $H_e(t)$ $[H(t)]$ versus t/T, where $J = 50/T$ is set for the full Hamiltonian $H(t)$. The red solid line: $P^{\rm eff}_{W'}(t)$; the blue dashed-dotted line: $P^{\rm full}_{W'}(t)$; the green dashed line: $P^{\rm eff}_{+}(t)$; and the purple dotted line: $P^{\rm full}_{+}(t)$.

With the designed control fields, the variations of populations of W state $|W'\rangle$ and GHZ state $|GHZ_+\rangle$ in time interval $[T, 2T]$ are also plotted in Fig. 2(b) with both effective Hamiltonian $H_e(t)$ and full Hamiltonian $H(t)$. The result also shows good matching between the effective dynamics and full dynamics. Moreover, the infidelity for the conversion from $|W'\rangle$ to $|{\rm GHZ}_+\rangle$ is $1 - P^{\rm full}_{+}(T) = 7.9262 \times 10^{-5}$. Therefore, the conversions between $|{\rm GHZ}_+\rangle$ and $|W'\rangle$ can be both accomplished with high fidelities.

3. The conversions between $|GHZ_-\rangle$ and $|W\rangle$

We now briefly discuss the conversions between $|{\rm GHZ}_-\rangle$ and $|W\rangle$. Based on Eq. (18) and the results of Sec. II C 1, to realize the conversions between $|{\rm GHZ}_-\rangle$ and $|W\rangle$, we just need to replace the parameter $\theta_4(t) = \pi/4$ in Sec. II C 1 by $\theta_4(t) = -\pi/4$. Assume the time interval for the conversion from $|{\rm GHZ}_-\rangle$ $(|W\rangle)$ to $|W\rangle$ $(|{\rm GHZ}_-\rangle)$ is $[0, T]([T, 2T])$, with the replacement, the variations of the control fields in time interval $[0, T]$ and the variations of population $P_W(t)$ of W state $|W\rangle$ and the population $P_-(t) = \langle {\rm GHZ}_-|\rho(t)|{\rm GHZ}_-\rangle$ of GHZ state $|{\rm GHZ}_-\rangle$ in time interval $[0, 2T]$ are plotted in Figs. 3(a) and 3(b), respectively. As shown by Fig. 3(b), the conversions between $|{\rm GHZ}_-\rangle$ and $|W\rangle$ can also be realized with the protocol successfully, and the infidelity for the conversion from $|{\rm GHZ}_-\rangle$ to $|W\rangle$ $(|W\rangle$ to $|{\rm GHZ}_-\rangle)$ is 7.9206×10^{-5} (7.8917×10^{-5}). In a similar way, to realize the conversions between $|{\rm GHZ}_-\rangle$ and $|W'\rangle$, one just needs to replace the parameter $\theta_4(t) = \pi/4$ in Sec. II C 2 by $\theta_4(t) = -\pi/4$. Thus, we here omit the detailed discussions about the conversions between $|{\rm GHZ}_-\rangle$ and $|W'\rangle$.

III. ANALYSIS OF EXPERIMENTAL ERRORS AND IMPERFECTIONS

In this section, let us make some discussions about experimental errors and imperfections. As an example, we consider the conversions from $|{\rm GHZ}_+\rangle$ to $|W\rangle$ and $|W'\rangle$ as examples in the following discussions. As it is hard to completely eliminate the influence of parametric errors, we should make some discussions about the performance of the protocol with errors being considered. Here, we first consider the systematic error of the control field $\Omega_j(t)$ $(j = 1, 2, 3)$. The erroneous control field with the systematic error reads

$$\Omega^{\rm se}_j(t) = (1 + \eta_j)\Omega_j(t), \tag{36}$$

with η_j being the amplitude of the systematic error of $\Omega_j(t)$. By numerically calculating the evolution with the perturbed

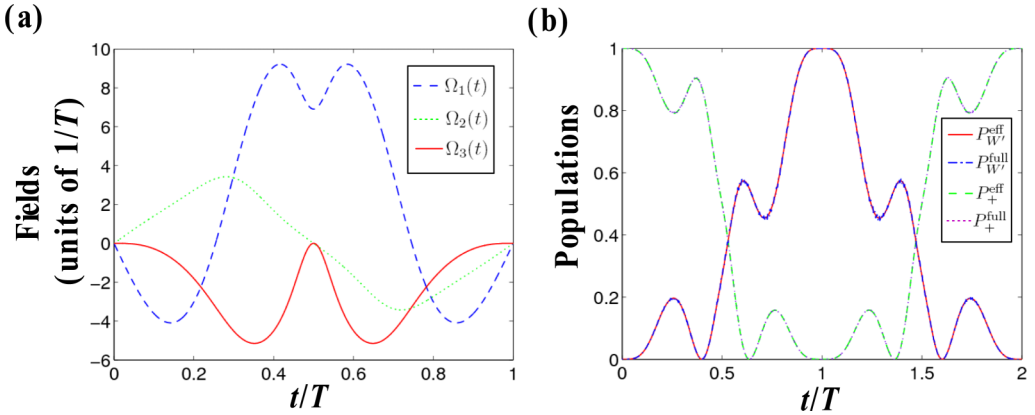

FIG. 3. (a) $\Omega_1(t)$, $\Omega_2(t)$, and $\Omega_3(t)$ versus t/T for $t \in [0, T]$. (b) The population $P^{\rm eff}_{W}(t)$ $[P^{\rm full}_{W}(t)]$ of W state $|W\rangle$ and the population $P^{\rm eff}_{-}(t)$ $[P^{\rm full}_{-}(t)]$ of GHZ state $|{\rm GHZ}_-\rangle$ with effective (full) Hamiltonian $H_e(t)$ $[H(t)]$ versus t/T, where $J = 50/T$ is set for the full Hamiltonian $H(t)$. The red solid line: $P^{\rm eff}_{W}(t)$; the blue dashed-dotted line: $P^{\rm full}_{W}(t)$; the green dashed line: $P^{\rm eff}_{-}(t)$; and the purple dotted line: $P^{\rm full}_{-}(t)$.

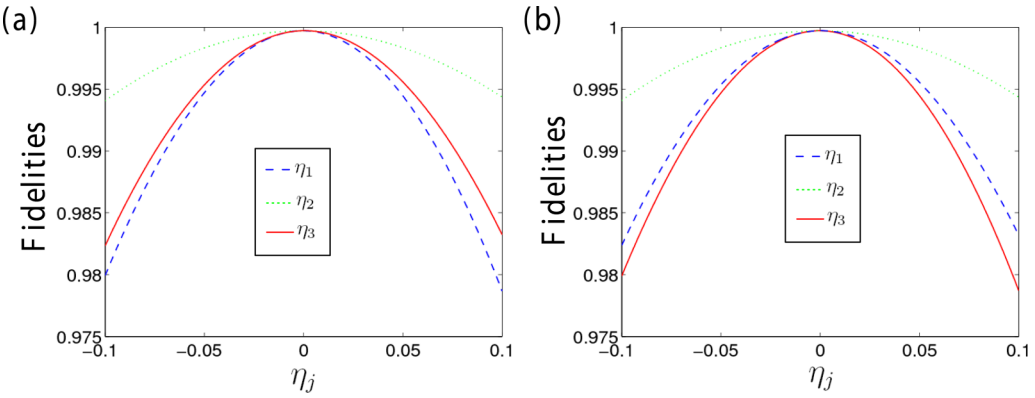

FIG. 4. (a) The fidelity of the conversion from $|\mathrm{GHZ}_+\rangle$ to $|W\rangle$ versus η_j ($j = 1, 2, 3$). (b) The fidelity of the conversion from $|\mathrm{GHZ}_+\rangle$ to $|W'\rangle$ versus η_j.

Hamiltonian, we plot the fidelities of the state conversions from $|\mathrm{GHZ}_+\rangle$ to $|W\rangle$ and $|W'\rangle$ versus η_j in Figs. 4(a) and 4(b), respectively. As shown by Figs. 4(a) and 4(b), the influence of the systematic error has positive correlation with the amplitude of the control field. For the conversion from $|\mathrm{GHZ}_+\rangle$ to $|W\rangle$, $\Omega_1(t)$ has the largest amplitude among $\{\Omega_j(t)\}$. Thus, the fidelity of the conversion is most sensitive to the systematic error of $\Omega_1(t)$. Similarly, for the conversion from $|\mathrm{GHZ}_+\rangle$ to $|W'\rangle$, as $\Omega_3(t)$ possesses the largest amplitude among $\{\Omega_j(t)\}$, the fidelity of the conversion is most sensitive to the systematic error of $\Omega_3(t)$. However, for both the conversions from $|\mathrm{GHZ}_+\rangle$ to $|W\rangle$ and $|W'\rangle$, the fidelities keep higher than 0.975 when each η_j of $\{\eta_j | j = 1, 2, 3\}$ varies from -10% to 10%. Therefore, the state conversions hold robustness against the systematic errors.

Second, let us investigate the influence of random noise to the state conversions. Different from the systematic error, the random noise is more unpredictable and usually shows different results in repeated experiments for the same state conversion process. Here, we try to estimate the robustness of the state conversions by adding additive white Gaussian noise (AWGN) to the control field $\Omega_j(t)$, which leads to the noisy control field as

$$\Omega_j^{\mathrm{no}}(t) = \Omega_j(t) + \mathrm{awgn}(\Omega_j(t), \kappa_j), \tag{37}$$

where $\mathrm{awgn}(\Omega_j(t), \kappa_j)$ denotes a function-generating AWGN with signal-to-noise ratio (SNR) κ_j for $\tilde{\Omega}_j(t)$. For both state conversions from $|\mathrm{GHZ}_+\rangle$ to $|W\rangle$ and $|W'\rangle$, we consider three groups of SNRs as $\kappa_j = 10$, $\kappa_j = 5$, and $\kappa_j = 1$. For each group of κ_j, we perform 15 repeated simulations to study the average effect caused by the AWGN, where the infidelities are plotted in Figs. 5(a) and 5(b), respectively, versus simulation counts. According to Figs. 5(a) and 5(b), when the AWGNs are added to the control fields, the infidelities for the conversions from $|\mathrm{GHZ}_+\rangle$ to $|W\rangle$ and $|W'\rangle$ are both higher than the results without the AWGN shown in Sec. II C 1 and II C 2, respectively. But the influence of AWGN is not very significant. As we can see from Figs. 5(a) and 5(b), when $\kappa_j = 10$ and $\kappa_j = 5$, the infidelities of the state conversions in the repeated simulations mostly range from 2×10^{-4} to 5×10^{-4}. Even when $\kappa_j = 1$, where the amplitude of the noise can reach the scale of the original control fields, the infidelities are still less than 10^{-3} in the 15 repeat simulations. The reason for the small influence of the AWGN is perhaps due to the fact that the time average of the AWGN is zero, and thus the pulse areas of the control fields are nearly unchanged even when the amplitude of AWGN reaches the scale of the original control fields. In the Appendix, we calculate the errors of pulse areas of $\Omega_1(t)$, $\Omega_2(t)$, and $\Omega_3(t)$ in the conversion from $|\mathrm{GHZ}_+\rangle$ to $|W\rangle$ in a single numerical simulation with

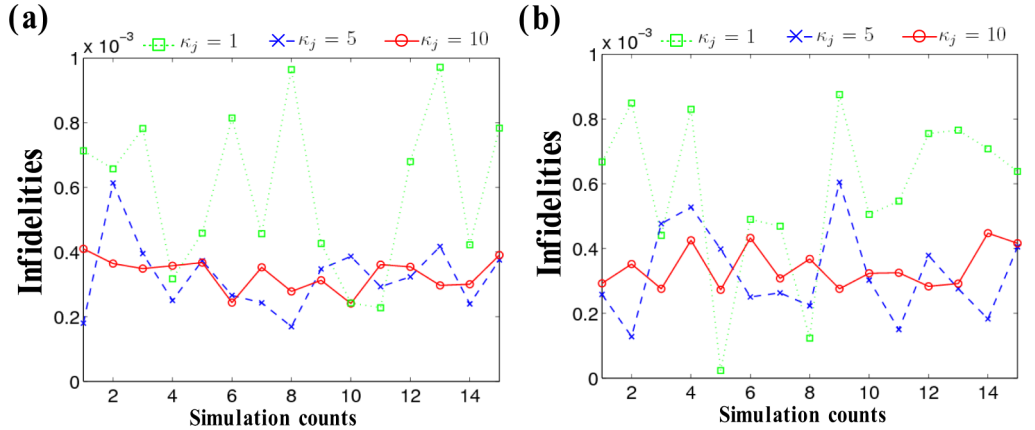

FIG. 5. (a) The infidelity of the conversion from $|\mathrm{GHZ}_+\rangle$ to $|W\rangle$ under AWGN versus simulation counts. (b) The infidelity of the conversion from $|\mathrm{GHZ}_+\rangle$ to $|W'\rangle$ under AWGN versus simulation counts.

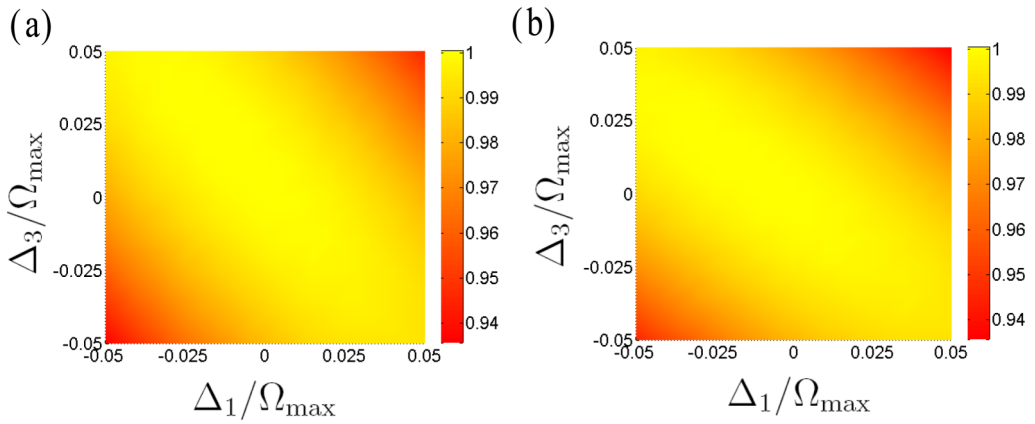

FIG. 6. (a) The fidelity of the conversion from $|\mathrm{GHZ}_+\rangle$ to $|W\rangle$ versus $\Delta_1/\Omega_{\max}$ and $\Delta_3/\Omega_{\max}$. (b) The fidelity of the conversion from $|\mathrm{GHZ}_+\rangle$ to $|W'\rangle$ versus $\Delta_1/\Omega_{\max}$ and $\Delta_3/\Omega_{\max}$.

AWGN and $\kappa_j = 1$ as an example to show that the errors of the pulse area are still very small when SNR is equal to 1. The results prove that the state conversions are robust against random noise.

Third, the frequency-matching conditions $\omega_1 = -12J$, $\omega_2 = 0$, $\omega_3 = 12J$ are also important to the current protocol. In experiments, there may exist small mismatching for the rotation frequencies of magnetic fields. It is worthwhile to investigate the influence of frequency mismatching to the state conversions. As ω_2 is set as zero, the direction of the magnetic component $B_2(t)$ is fixed along y axis with $\phi_2 = -\pi/2$. Thus, we only discuss the mismatching of ω_1 and ω_3 as $\Delta_1 = \omega_1^e - \omega_1$ and $\Delta_3 = \omega_3^e - \omega_3$, with ω_1^e and ω_3^e being the erroneous rotation frequencies for magnetic components $B_1(t)$ and $B_3(t)$, respectively. Besides, to compare the scales of Δ_1 and Δ_3 with the amplitudes of $\Omega_j(t)$, we define $\Omega_{\max} = \max_{0\leqslant t\leqslant T}\{\Omega_j(t)|j = 1, 2, 3\}$, and plot the fidelities of the conversions from $|\mathrm{GHZ}_+\rangle$ to $|W\rangle$ and $|W'\rangle$ versus $\Delta_1/\Omega_{\max}$ and $\Delta_3/\Omega_{\max}$ in Figs. 6(a) and 6(b), respectively. Seen from Figs. 6(a) and 6(b), the fidelities of the state conversions from $|\mathrm{GHZ}_+\rangle$ to $|W\rangle$ and $|W'\rangle$ are both higher than 0.935 when $|\Delta_1/\Omega_{\max}|, |\Delta_3/\Omega_{\max}| \leqslant 5\%$. Thus, the state conversions possess robustness against small mismatching of the rotation frequencies of magnetic fields. Besides, when Δ_1 and Δ_3 have different signs, the fidelities remain almost unchanged, while in the case where Δ_1 and Δ_3 have the same sign, the fidelities are more sensitive to the variations of Δ_1 and Δ_3. Therefore, in experiments, one should try to avoid the case where Δ_1 and Δ_3 have the same sign.

IV. DISCUSSIONS AND CONCLUSIONS

In conclusion, a protocol was proposed to realize the conversions between GHZ states $|\mathrm{GHZ}_\pm\rangle$ and W states $|W\rangle, |W'\rangle$ for spin qubits via the inverse Hamiltonian engineering based on Lie transforms. First, we derived the effective Hamiltonian $H_e(t)$ by selecting suitable rotation frequencies of the components of magnetic fields. Then, based on the derived effective Hamiltonian $H_e(t)$, the dynamic symmetry was analyzed, and the initial phase for each component of the magnetic fields was determined, such that the Hamiltonian and the evolution of the system can be considered within SO(4) Lie algebra. After that, by using the Lie-transform-based inverse Hamiltonian engineering, the expressions of the control fields and the corresponding constraint equations of parameters were given. To show the validity of the effective dynamics and the control fields, three examples of the state conversions were studied, where the fidelities of the state conversions are all nearly unities. Finally, the influences of the systematic errors, random noise, and frequency mismatching were also investigated by numerical simulations. The results show the protocol possesses the robustness when these disturbing factors are taken into account.

Apart from the robustness, the protocol also holds some other advantages. First, with the effective Hamiltonian and the Lie-transform-based Hamiltonian engineering, multitype state conversions can be realized in one step. More specifically, we can see from Eq. (18) that, besides the examples considered in the Sec. II C, the conversions between GHZ states $|\mathrm{GHZ}_+\rangle$ and $|\mathrm{GHZ}_-\rangle$, and that between W states $|W\rangle$ and $|W'\rangle$ are also possible. Moreover, we can also generate the four types of entangled states $|\mathrm{GHZ}_+\rangle$, $|\mathrm{GHZ}_-\rangle$, $|W\rangle$, and $|W'\rangle$ from product states $|\uparrow\uparrow\uparrow\rangle$ and $|\downarrow\downarrow\downarrow\rangle$ via the protocol. Furthermore, according to Eq. (17), with the evolution operator being given, the implementation of the three-qubit controlled phase gate is also available. For example, we can set the boundary conditions as $\theta_j(0) = 0\,(j = 1, 2, 3, \ldots, 6)$ and

$$\theta_1(T) = \theta_3(T) = \theta_5(T) = \theta_6(T) = \pi,$$
$$\theta_2(T) = \theta_4(T) = 0. \tag{38}$$

Then the evolution operator at $t = T$ becomes $U(T) = \mathbb{1} - 2|\downarrow\downarrow\downarrow\rangle\langle\downarrow\downarrow\downarrow|$ in the rotation frame of e^{-iH_0t} ($\mathbb{1}$ denotes the identity operator). By selecting a proper interaction time T to eliminate the phase shift resulting from the H_0, the three-qubit controlled phase gate can be realized. These points mentioned above may be open questions for the investigations afterward.

Second, the state conversions in the protocol are all deterministic and reversible. Different from the previous probabilistic protocols [19,23], the physical resources that may be wasted in the failed cases can be saved. On the other hand, compared with previous protocols using the homodyne measurement [24] and the dissipative dynamics process [25],

where the state conversions are both one way, the current protocol is more flexible in applications. Therefore, if necessary, one can turn the GHZ state to the W state, then turn it back without preparing the source state again, which can also save physical resources.

Third, since the magnetic field applied on each spin qubit and the coupling strengths between each pair of spin qubits are all set to be equal, it is unnecessary to address and manipulate spin qubits individually. Thus, the control of the system is global, which may relax the experimental requirements.

With the advantages mentioned above, we hope the protocol can benefit the fundamental research of quantum mechanics and the applications of QIP based on the GHZ states and the W states.

ACKNOWLEDGMENTS

This work was supported by the National Natural Science Foundation of China under Grants No. 11575045, No. 11374054, No. 11674060, No. 2018J01414, and No. 11805036.

APPENDIX : THE INFLUENCE OF THE AWGN TO THE PULSE AREAS

We now show that the AWGN influences the pulse area of the control field $\Omega_j(t)$ slightly even when SNR is 1. Before starting the discussion, we first give the definitions of the pulse area of $\Omega_j(t)$ and its error under the influence of AWGN with SNR $\kappa_j = 1$ as

$$\mathcal{A}_j = \int_0^T \Omega_j(t)dt \tag{A1}$$

and

$$\delta\mathcal{A}_j = \int_0^T [\Omega_j^{\rm no}(t) - \Omega_j(t)]dt = \int_0^T \mathrm{awgn}(\Omega_j(t), 1)dt, \tag{A2}$$

respectively. We perform a single simulation and plot the fidelity of the conversion from $|\mathrm{GHZ}_+\rangle$ to $|W\rangle$ versus t/T with AWGN and $\kappa_j = 1$ in Fig. 7(a). Besides, $\Omega_j^{\rm no}(t)$ and $\mathrm{awgn}(\Omega_j(t), 1)$ versus t/T are plotted in Fig. 7(b_1–b_3). As shown by Fig. 7(a), the variation of the fidelity under the influence of AWGN is very similar to that without AWGN [see Fig. 1(c)]. The infidelity of the conversion from $|\mathrm{GHZ}_+\rangle$ to $|W\rangle$ is 1.5746×10^{-4} at $t = T$. On the other hand, by comparing the variation of $\Omega_j^{\rm no}(t)$ in Fig. 7(b_j) with that of $\Omega_j(t)$ shown in Fig. 1(b), we find that the shape of the wave envelope of $\Omega_j^{\rm no}(t)$ is similar to $\Omega_j(t)$. Moreover, one can also find that the time average of $\mathrm{awgn}(\Omega_j(t), 1)$ is near zero from Fig. 7(b_j). We calculate the error of the pulse area of $\Omega_j(t)$ according to Eq. (A2). The result is $\delta\mathcal{A}_1 = 0.0049$, $\delta\mathcal{A}_2 = 0.0144$, and $\delta\mathcal{A}_3 = -0.0096$. Considering the fact that the infidelity of the evolution is proportional to the square of the pulse area for a transition between two levels, we calculate the value $\delta\mathcal{A}_1^2 + \delta\mathcal{A}_2^2 + \delta\mathcal{A}_3^2 = 3.2440 \times 10^{-4}$, which is on

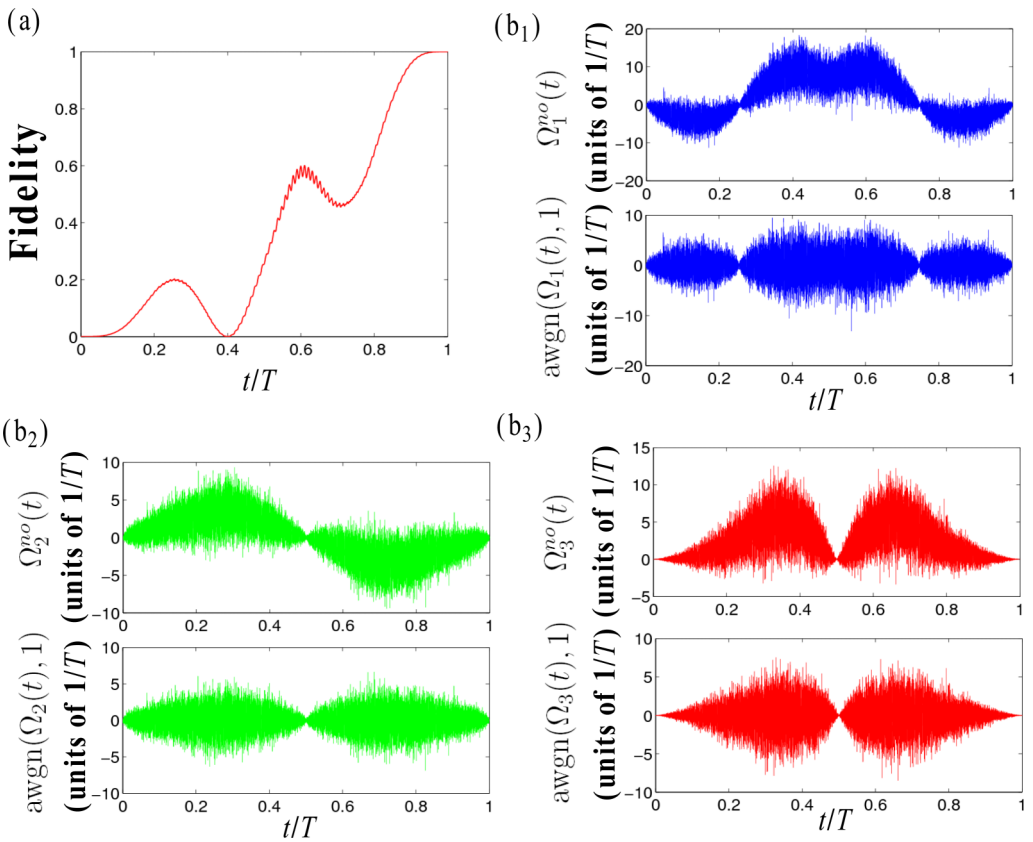

FIG. 7. (a) The fidelity of the conversion from $|\mathrm{GHZ}_+\rangle$ to $|W\rangle$ versus t/T with AWGN and $\kappa_j = 1$. (b_1) $\Omega_1^{\rm no}(t)$ and $\mathrm{awgn}(\Omega_1(t), 1)$ versus t/T. (b_2) $\Omega_2^{\rm no}(t)$ and $\mathrm{awgn}(\Omega_2(t), 1)$ versus t/T. (b_3) $\Omega_3^{\rm no}(t)$ and $\mathrm{awgn}(\Omega_3(t), 1)$ versus t/T.

the same order of the infidelity shown above. Thus, the errors of the pulse areas are still small when the AWGN reach the scale of the original pulses. As a result, the infidelity of the conversion is also small.

[1] C. H. Bennett and D. P. DiVincenzo, Nature (London) **404**, 247 (2000).
[2] S. L. Braunstein and H. J. Kimble, Phys. Rev. Lett. **80**, 869 (1998).
[3] A. K. Ekert, Phys. Rev. Lett. **67**, 661 (1991).
[4] D. P. Divincenzo, Science **270**, 255 (1995).
[5] Z. X. Man, Y. J. Xia, and N. B. An, Phys. Rev. A **78**, 064301 (2008).
[6] L. Xiao, G. L. Long, F. G. Deng, and J. W. Pan, Phys. Rev. A **69**, 052307 (2004).
[7] D. M. Greenberger, M. A. Horne, and A. Zeilinger, in *Bell's Theorem, Quantum Theory, and Conceptions of the Universe*, edited by M. Kafatos (Kluwer, Dordrecht, 1989), p. 69.
[8] W. Dür, G. Vidal, and J. I. Cirac, Phys. Rev. A **62**, 062314 (2000).
[9] A. Cabello, Phys. Rev. A **65**, 032108 (2002).
[10] S. B. Zheng, Phys. Rev. A **66**, 014103 (2002).
[11] E. Jung, M. R. Hwang, Y. H. Ju, M. S. Kim, S. K. Yoo, H. Kim, D. K. Park, J. W. Son, S. Tamaryan, and S. K. Cha, Phys. Rev. A **78**, 012312 (2008).
[12] A. Karlsson and M. Bourennane, Phys. Rev. A **58**, 4394 (1998).
[13] M. Hillery, V. Bužek, and A. Berthiaume, Phys. Rev. A **59**, 1829 (1999).
[14] A. M. Lance, T. Symul, W. P. Bowen, B. C. Sanders, and P. K. Lam, Phys. Rev. Lett. **92**, 177903 (2004).
[15] T. Gao, F. L. Yan, and Z. X. Wang, J. Phys. A: Math. Gen. **38**, 5761 (2005).
[16] X. R. Jin, X. Ji, Y. Q. Zhang, S. Zhang, S. K. Hong, K. H. Yeon, and C. I. Um, Phys. Lett. A **354**, 67 (2006).
[17] M. J. Zhao, Phys. Rev. A **91**, 012310 (2015).
[18] A. Miyake, Phys. Rev. A **67**, 012108 (2003).
[19] P. Walther, K. J. Resch, and A. Zeilinger, Phys. Rev. Lett. **94**, 240501 (2005).
[20] A. Acín, D. Bruß, M. Lewenstein, and A. Sanpera, Phys. Rev. Lett. **87**, 040401 (2001).
[21] T. Tashima, M. S. Tame, Ş. K. Özdemir, F. Nori, M. Koashi, and H. Weinfurter, Phys. Rev. A **94**, 052309 (2016).
[22] H. F. Wang, S. Zhang, A. D. Zhu, X. X. Yi, and K. H. Yeon, Opt. Express **19**, 25433 (2011).
[23] G. Y. Wang, D. Y. Wang, W. X. Cui, H. F. Wang, A. D. Zhu, and S. Zhang, J. Phys. B **49**, 065501 (2016).
[24] W. X. Cui, S. Hu, H. F. Wang, A. D. Zhu, and S. Zhang, Opt. Express **24**, 15319 (2016).
[25] J. Song, X. D. Sun, Q. X. Mu, L. L. Zhang, Y. Xia, and H. S. Song, Phys. Rev. A **88**, 024305 (2013).
[26] T. Gaebel, M. Domhan, I. Popa, C. Wittmann, P. Neumann, F. Jelezko, J. R. Rabeau, N. Stavrias, A. D. Greentree, S. Prawer, J. Meijer, J. Twamley, P. R.'Hemmer, and J. Wrachtrup, Nat. Phys. **2**, 408 (2006).
[27] C. H. van der Wal, A. C. J. ter Haar, F. K. Wilhelm, R. N. Schouten, C. J. P. M. Harmans, T. P. Orlando, S. Lloyd, and J. E. Mooij, Science **290**, 773 (2000).
[28] S. Oh, L. A. Wu, Y. P. Shim, J. Fei, M. Friesen, and X. Hu, Phys. Rev. A **84**, 022330 (2011).
[29] S. Bose, Phys. Rev. Lett. **91**, 207901 (2003).
[30] Z. L. Xiang, S. Ashhab, J. Q. You, and F. Nori, Rev. Mod. Phys. **85**, 623 (2013).
[31] K. Korzekwa, P. Machnikowski, and P. Horodecki, Phys. Rev. A **89**, 062301 (2014).
[32] P. Karbach and J. Stolze, Phys. Rev. A **72**, 030301(R) (2005).
[33] D. Culcer, Ł. Cywiński, Q. Li, X. Hu, and S. Das Sarma, Phys. Rev. B **82**, 155312 (2010).
[34] J. J. Pla, K. Y. Tan, J. P. Dehollain, W. H. Lim, J. J. L. Morton, F. A. Zwanenburg, D. N. Jamieson, A. S. Dzurak, and A. Morello, Nature **496**, 334 (2013).
[35] C. B. Simmons, J. R. Prance, B. J. Van Bael, T. S. Koh, Z. Shi, D. E. Savage, M. G. Lagally, R. Joynt, M. Friesen, S. N. Coppersmith, and M. A. Eriksson, Phys. Rev. Lett. **106**, 156804 (2011).
[36] C. Pagonis and R. Clifton, Phys. Lett. A **168**, 100 (1992).
[37] L. Hardy, Phys. Rev. Lett. **71**, 1665 (1993).
[38] K. Paul and A. K. Sarma, Phys. Rev. A **94**, 052303 (2016).
[39] D. Stefanatos and E. Paspalakis, Phys. Rev. A **99**, 022327 (2019).
[40] X. T. Yu, Q. Zhang, Y. Ban, and X. Chen, Phys. Rev. A **97**, 062317 (2018).
[41] S. Oh, Y. P. Shim, J. Fei, M. Friesen, and X. Hu, Phys. Rev. A **87**, 022332 (2013).
[42] R. R. Agundez, C. D. Hill, L. C. L. Hollenberg, S. Rogge, and M. Blaauboer, Phys. Rev. A **95**, 012317 (2017).
[43] B. H. Huang, Y. H. Kang, Y. H. Chen, Z. C. Shi, J. Song, and Y. Xia, Phys. Rev. A **97**, 012333 (2018).
[44] S. B. Zheng, Phys. Rev. A **87**, 042318 (2013).
[45] D. Jaksch, C. Bruder, J. I. Cirac, C. W. Gardiner, and P. Zoller, Phys. Rev. Lett. **81**, 3108 (1998).
[46] D. Porras and J. I. Cirac, Phys. Rev. Lett. **92**, 207901 (2004).
[47] A. Micheli, G. K. Brennen, and P. Zoller, Nat. Phys. **2**, 341 (2006).
[48] T. Chen, J. Zhang, and Z. Y. Xue, Phys. Rev. A **98**, 052314 (2018).
[49] Z. Y. Xue, J. Zhou, Y. M. Chu, and Y. Hu, Phys. Rev. A **94**, 022331 (2016).
[50] Z. Y. Xue, J. Zhou, and Z. D. Wang, Phys. Rev. A **92**, 022320 (2015).
[51] E. Torrontegui, S. Ibáñez, X. Chen, A. Ruschhaupt, D. Guéry-Odelin, and J. G. Muga, Phys. Rev. A **83**, 013415 (2011).
[52] N. V. Vitanov, Phys. Rev. A **85**, 032331 (2012).
[53] U. Güngördü, Y. Wan, M. A. Fasihi, and M. Nakahara, Phys. Rev. A **86**, 062312 (2012).
[54] B. Rousseaux, S. Guerin, and N. V. Vitanov, Phys. Rev. A **87**, 032328 (2013).
[55] E. Torrontegui, S. Martínez-Garaot, and J. G. Muga, Phys. Rev. A **89**, 043408 (2014).
[56] S. Martínez-Garaot, E. Torrontegui, X. Chen, and J. G. Muga, Phys. Rev. A **89**, 053408 (2014).
[57] D. Guéry-Odelin and J. G. Muga, Phys. Rev. A **90**, 063425 (2014).

[58] Y. H. Chen, Y. Xia, Q. C. Wu, B. H. Huang, and J. Song, Phys. Rev. A **93**, 052109 (2016).
[59] B. J. Liu, Z. H. Huang, Z. Y. Xue, and X. D. Zhang, Phys. Rev. A **95**, 062308 (2017).
[60] Y. H. Kang, Y. H. Chen, Z. C. Shi, J. Song, and Y. Xia, Phys. Rev. A **94**, 052311 (2016).
[61] Y. H. Kang, Y. H. Chen, Z. C. Shi, B. H. Huang, J. Song, and Y. Xia, Phys. Rev. A **96**, 022304 (2017).
[62] Y. C. Li, D. Martínez-Cercós, S. Martínez-Garaot, X. Chen, and J. G. Muga, Phys. Rev. A **97**, 013830 (2018).
[63] Y. H. Kang, Y. H. Chen, Z. C. Shi, B. H. Huang, J. Song, and Y. Xia, Phys. Rev. A **97**, 042336 (2018).
[64] Y. H. Kang, Y. H. Chen, Z. C. Shi, B. H. Huang, J. Song, and Y. Xia, Phys. Rev. A **97**, 033407 (2018).
[65] X. Chen and J. G. Muga, Phys. Rev. A **86**, 033405 (2012).
[66] A. del Campo and M. G. Boshier, Sci. Rep. **2**, 648 (2012).
[67] X. Wang, L. S. Bishop, J. P. Kestner, E. Barnes, K. Sun, and S. D. Sarma, Nat. Commun. **3**, 997 (2003).
[68] Y. Ji, J. Bian, X. Chen, J. Li, X. Nie, H. Zhou, and X. Peng, Phys. Rev. A **99**, 032323 (2019).